

# Metasurface Superstrate-based MIMO Patch Antennas with Reduced Mutual Coupling for 5G Communications

Sthembile P. Dubazane, Pradeep Kumar, and Thomas J. O. Afullo

Discipline of Electrical, Electronic and Computer Engineering  
University of KwaZulu-Natal, Durban 4041, South Africa  
213526437@stu.ukzn.ac.za, pkumar\_123@yahoo.com, afullo@ukzn.ac.za

**Abstract** – Multiple-input multiple-output (MIMO) systems have several advantages, such as providing high capacity, spatial diversity, etc. MIMO antennas suffer with high mutual coupling (m-coupling) between the ports. In this paper, the metasurface with negative permeability (MNG) is designed and utilized for m-coupling reduction of a two-port rectangular microstrip MIMO antenna (Antenna 1). Two metasurface superstrate-based MIMO antennas with reduced m-coupling for fifth generation (5G) are proposed. The first design (Antenna 2) is constructed using a single metasurface superstrate suspended above the two-port MIMO microstrip antenna. The second design (Antenna 3) is constructed using a double metasurface superstrate layers suspended above the two-port MIMO microstrip antenna. Both metasurface-based MIMO antennas achieve significant m-coupling reduction over the entire bandwidth. The edge-to-edge separation between the two patches is  $0.29\lambda_0$ . The proposed Antenna 3 obtains the reduced m-coupling of  $-44$  dB along with the wide bandwidth of 5.92 – 6.2 GHz and a maximum gain of 6.79 dB. The proposed antennas are suitable for extended sub-6 GHz 5G applications with the operating frequency band of 5.9–6.1 GHz.

**Index Terms** – Permeability, permittivity, metasurface, mutual coupling.

## I. INTRODUCTION

Multiple-input multiple-output (MIMO) systems refer to the systems where the transmitting end and the receiving end are equipped with the multiple antenna elements. The use of multiple antennas results in significant increase in channel capacity, higher spectral efficiency, and reduced fading without requiring additional bandwidth and transmission power. Hence, the most modern wireless devices are anticipated to employ MIMO technology in wireless communication systems. For low correlation and suitable isolation, a distance of at least  $0.5\lambda_0$  (where  $\lambda_0$  is the free space wavelength at the operating frequency) is required between antenna

elements [1]. Due to miniaturization of most modern wireless devices, compact and dense antenna systems with much smaller distances are preferred, which results in high m-coupling between the antenna elements. M-coupling is generally as a result of surface waves or radiated waves and it degrades the antenna performance by deteriorating the radiation characteristics of the antenna system.

To reduce m-coupling, several decoupling methods or techniques have been proposed, which include, but are not limited to, electromagnetic band-gap (EBG) structures [2], defected ground structures (DGS) [3], metamaterials structures [4], decoupling networks [5], etc. The major drawback of these techniques are that these are mostly three dimensional structures; hence, they introduce fabrication difficulties and high cost. In this paper, a planar two-dimensional metasurface is used for m-coupling reduction. Metasurface is two-dimensional structure with properties equivalent to metamaterials. Metasurface structures are planar, thin, and practical for implementation; hence, they have been getting antenna researchers' attention in the recent years.

Various techniques have been used to reduce m-coupling between the antenna elements. Employment of decoupling networks (DNs) is one of the methods that have been highly utilized for m-coupling reduction. They work on the principle of transforming cross-admittance to a completely imaginary value by utilizing discrete elements and step-up transmission lines [6–11]. In [7], a coupled resonator decoupling method is used to decouple the coupled dual-band antennas. In the lower band (2.4 – 2.48 GHz), a maximum m-coupling reduction of 7 dB was achieved, while for the upper band (5.15 – 5.135 GHz), the m-coupling remains the same and is not reduced. In [9], an LTE700/WWAN MIMO antenna system is decoupled using a DN which consists of a suspended transmission line with two terminals shorted to the ground and a capacitor loaded at the center of the line. In the lower band (704 – 960 MHz), the m-coupling was reduced by 9 dB, while in the

upper band (1710 – 2170 MHz), the m-coupling was not reduced.

One of the other highly used techniques for m-coupling reduction is by the employment of EBG structures. The EBG structures are formed by a periodic arrangement of dielectric and metallic elements. The EBG structure can either block electromagnetic waves at specific frequencies or provide a medium to pass and transmit electromagnetic waves [12]. The most commonly used EBG structure for m-coupling reduction is the mushroom-like EBG structure [13–20]. In [14], the mushroom-like EBG structure was introduced between the two monopole antennas. A maximum m-coupling reduction of 13.4 dB was achieved.

In [15], a planar compact EBG structure was introduced between the two square microstrip patches with an edge-to-edge separation  $0.75\lambda_0$  for achieving a maximum m-coupling reduction of 6 dB. The major drawbacks with EBG structures are that they can be largely associated with the fabrication complexities due to their vertical via placement. Moreover, they require thicker substrates, which results in an increase in size of antenna structure.

DGS is another m-coupling reduction technique that is widely employed. It introduces periodic or non-periodic slits or defects on the antenna's ground plane to suppress the ground current between the antenna elements. Different DGS structural arrangements have been used to reduce m-coupling in different antenna arrays [21–27]. In [22], a dumbbell-like DGS was inserted between two multiband microstrip antenna array elements. A maximum m-coupling reduction of 6 dB was achieved. In [24], a slit pattern without a via was etched on the ground plane between two PIFA antennas with an edge-to-edge separation of  $0.116\lambda_0$ . A maximum m-coupling reduction of 10 dB was achieved. The main disadvantage of utilizing DGS for m-coupling reduction is that a segment of the propagating energy is leaked, which leads to the electromagnetic interference with the adjacent circuitry. Moreover, the introduced defect might lead to a distorted radiation pattern of the antenna structure.

The last technique that will be discussed is the employment of metamaterial structures to reduce m-coupling between the antenna elements. The usage of metamaterial structures for m-coupling reduction has grown popular over the years due to their ability to manipulate electromagnetic waves [28–33]. In [29], a spiral metamaterial resonator was printed on the microstrip antenna substrate between the two array elements. A maximum m-coupling reduction of 5.5 dB was achieved. In [32], a 3D dual-band metamaterial array structure was loaded on the top of a dual-band microstrip antenna array for m-coupling reduction. A maximum

m-coupling reduction of 3 dB was achieved. The major drawback of using metamaterials for m-coupling reduction is that they are frequently used as 3D structures, which introduces problems in terms of fabrication complexity and high cost. In most recent designs, where metasurface is employed for m-coupling reduction in array antenna systems, antenna mismatches can be seen. This then requires further antenna matching techniques to be utilized for improving antenna parameters and fabrication difficulties.

In this paper, the design, simulation, fabrication, and measurement of the metasurface-based antennas are presented. Two metasurface-based antennas, i.e., Antenna 2 and Antenna 3 are presented and their results are analyzed. The first design, i.e., Antenna 2 is achieved by suspending a single metasurface substrate on the top of the microstrip antenna, while the second design, i.e., Antenna 3 is achieved by suspending a double metasurface substrate on the top of the microstrip antenna.

## II. DESIGN AND GEOMETRY OF METASURFACE-BASED MIMO ANTENNAS

Two metasurface superstrate-based antennas are presented in this paper. The proposed designs utilize the MNG metasurface which is equivalent to the medium with negative permeability. The metasurface is designed using periodic split ring resonators (SRR). The MNG metasurface is designed such that it rejects wave propagation at the center frequency and, hence, reduces the m-coupling between the antenna elements. The first design employs a single metasurface superstrate suspended over the radiating antenna elements. In this design, the m-coupling is reduced from  $-29$  to  $-61$  dB, while the gain is significantly reduced from 4.79 to 1.69 dB. The second design employs a double metasurface superstrate suspended over the radiating antenna elements. In this design, the m-coupling between the antenna elements is reduced from  $-24$  to  $-46$  dB, while the gain is increased from 4.71 to 6.79 dB.

### A. Antenna 1

To demonstrate the effectiveness of the metasurface superstrate-based antenna designs, a two-element MIMO rectangular microstrip antenna is designed. This antenna is designed using the transmission line model of analysis. The antennas for MIMO systems require separate feeding for every antenna element [34, 35]. The antenna structure is simulated and optimized using the CST Microwave Studio. This antenna is designed for the resonant frequency of 6 GHz in the sub-6 GHz band. Sub-6 GHz band is the frequency range below 6 GHz and is defined as frequency range 1 (FR1) in fifth generation (5G) technology for various ISM applications [36, 37]. Recently, some antennas have been designed for sub-6 GHz applications 38–40.

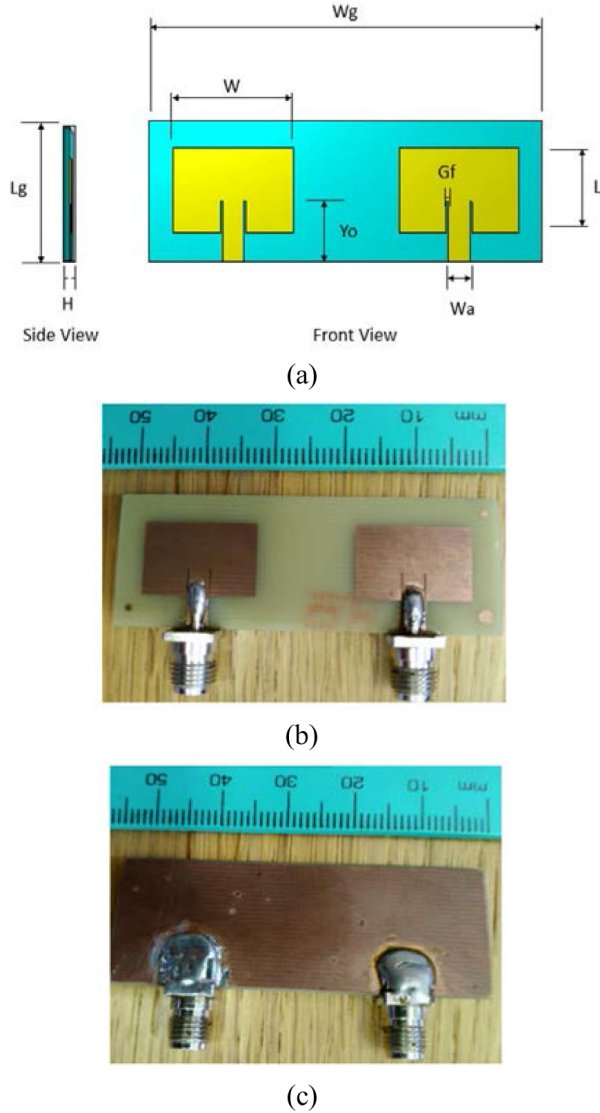


Fig. 1. Two-port MIMO microstrip antenna (Antenna 1). (a) Antenna configuration. (b) Top view of fabricated Antenna 1. (c) Bottom view of fabricated Antenna 1.

The 5G frequency bands are regularly updated and new bands are availed in different countries. Recently the 3rd Generation Partnership Project (3GPP) extended the 5G FR1 band from (410 MHz – 6 GHz) to (410 MHz – 7.125 GHz), hence introducing 1200 MHz additional spectrum [41]. In 2020, the Federal Communication Commission (FCC) also permitted the usage of 6 GHz band (5.925–7.125 GHz) for unlicensed use. This was done with certain regulations and standards to protect incumbent licensed services from interference [42–45]. This approval of 6 GHz for unlicensed use has introduced a new market for 6 GHz wireless solutions like the new Wi-Fi 6E which is an extension for Wi-Fi 6 which operates at the (2.4 and 5 GHz) bands [42].

Table 1: Dimensional parameters of the MIMO antenna and the metasurface unit cell

Parameter	Value (mm)	Parameter	Value (mm)
$W_g$	55	$W_{gm}$	7.844
$L_g$	20.382	$L_{gm}$	7.844
$W$	16.3	$W_{m1}$	5.06
$L$	11.3822	$L_{m1}$	5.06
$W_a$	2.89	$W_{m2}$	2
$Y_o$	4.2112	$G_1$	1
$G_f$	0.083781	$G_2$	0.5
$H$	1.5	$H$	1.5
$W_s$	65	$H_{s1}$	6.5
$L_s$	33.862	$H_{s2}$	3

The two-port MIMO rectangular microstrip antenna is depicted in Figure 1. It is printed on an FR-4 substrate with a dielectric constant of 4.4, a loss tangent of 0.002, and a substrate thickness of 1.5 mm. The top view and bottom view of fabricated Antenna 1 are shown in Figures 1 (b) and (c), respectively. The thickness of the copper layer is 0.035 mm. The dimensional parameters of the antenna and metasurface unit cell are listed in Table 1.

## B. Metasurface

The dielectric properties of the dielectric material can be utilized to improve the performance of the microstrip antenna [46, 47]. Metasurface-based antenna designs have been previously utilized [48–52]. In [51], a metasurface superstrate is suspended above an antenna array for m-coupling reduction purposes. A mutual coupling reduction of 19 dB is achieved. In [52], a metasurface superstrate is also utilized to reduce the m-coupling of an antenna array. Maximum m-coupling reduction of 25 dB is achieved. In both designs, the employment of metasurface superstrates results in significant antenna mismatches. In [51], when the metasurface superstrate is employed, the reflection coefficient is significantly increased from  $-30$  to  $-9$  dB, while in [52], the reflection coefficient is increased from  $-20$  to  $-5$  dB. To combat the antenna mismatches, a U-shaped slot was etched on all elements of the antenna array. However, introducing the slots to an antenna changes the path of the current distribution which can result in changes in radiation patterns and impedance. Additionally, the introduction of the U-slot increases fabrication cost and complexities. The design conducted in this paper does not require additional matching methods, which means that it is inexpensive to fabricate and the structure is less complex. In addition to that, this design can be implemented in already existing antenna designs because it does not change the original structure of the antenna.

The decoupling metasurface is designed using SRR to achieve a negative permeability medium. They are

formed by a pair of metal loops printed on a dielectric substrate with gaps or slits  $180^\circ$  from each other. The split gap between the rings results in a capacitance, while the metal loops result in an inductance, hence forming an  $LC$  circuit. This  $LC$  circuit is responsible for producing the resonant frequency of the metasurface, while the magnetic field induced in SRR is responsible for creating negative permeability. The metasurface unit cell is depicted in Figure 2. It consists of lossless copper loops printed on an FR-4 substrate with dielectric constant of 4.4, a thickness of 1.5 mm, and a loss tangent of 0.002. The optimized dimensions of the unit cell are listed in Table 1.

The negative frequency region and the resonant frequency of the designed SRR unit cell are as the result of the physical dimensions of the ring and the size of the slip gap between the rings. During the design and optimization of the unit cell, the dimensions of the rings and split gaps are varied to obtain the desired resonant frequency, permeability, and permittivity. In this design, the optimization parameters are selected to be  $G1$  and  $G2$ . The real and imaginary values of permittivity ( $\epsilon$ ) and permeability ( $\mu$ ) of the SRR unit cell are extracted using

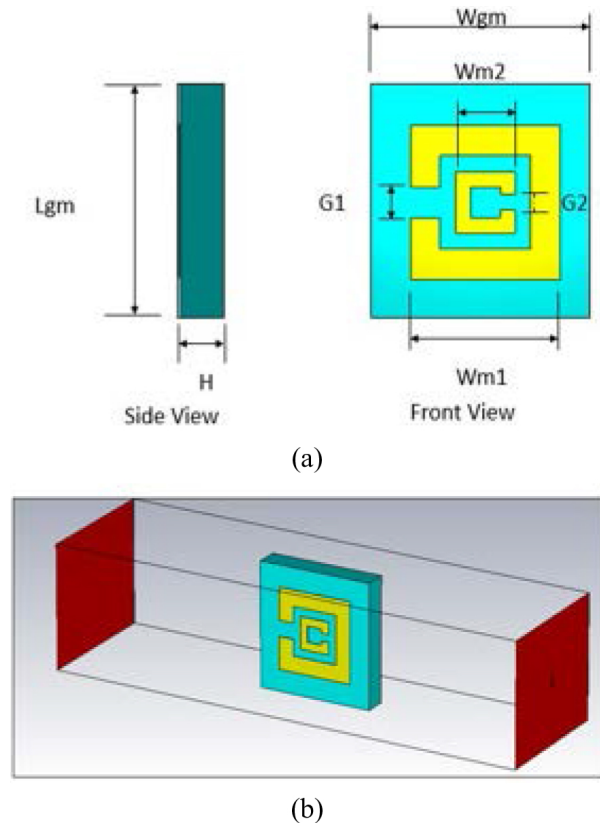


Fig. 2. Metasurface unit cell. (a) Geometry. (b) CST simulation model.

CST Microwave Studio. However, the real parts are the ones of significant concern in this design. Figure 3 depicts the real part of permittivity and permeability. It can be observed that the real part of permeability is negative in the 6-GHz frequency range, while the real part of permittivity is positive in the same frequency range. The real part of permeability while varying split gap 1 ( $G1$ ) is depicted in Figure 4. From Figure 4, it can be observed that varying  $G1$  changes the resonant frequency as well as the permeability of the unit cell. The designed metasurface is used in the reference microstrip antenna; it introduces the region with negative permeability and positive permittivity.

In this region, the wave number is given by [51, 52]

$$k = k_o \cdot \sqrt{-|\mu_r| \cdot |\epsilon_r|} = jk_o \cdot \sqrt{|\mu_r| \cdot |\epsilon_r|}. \quad (1)$$

From eqn (1), it can be observed that  $k$  is purely imaginary, resulting in the electric field of the  $x$ -component

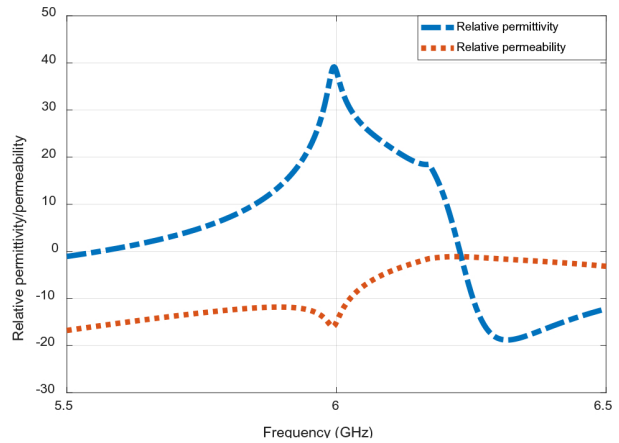


Fig. 3. Relative permittivity ( $\epsilon_r$ ) and relative permeability ( $\mu_r$ ) of the metasurface unit cell.

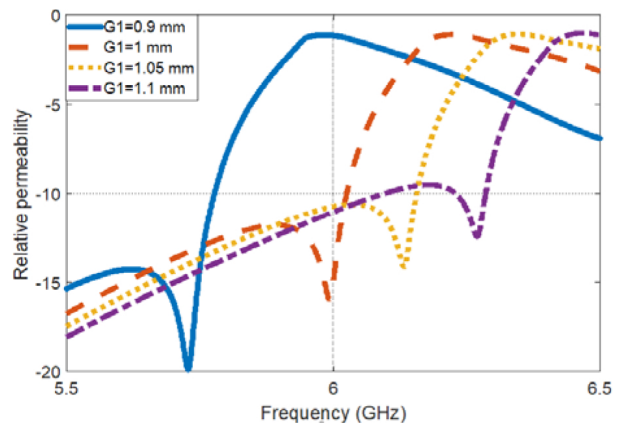


Fig. 4. Real part of permeability with different values of  $G1$ .

$(A_0 e^{jkx})$  to be expressed as [51, 52]

$$A_0 e^{jkx} \cdot e^{j\omega t} = A_0 e^{j(k_0 \cdot \sqrt{|\mu_r| \cdot |\epsilon_r|})x} \cdot e^{j\omega t}, \quad (2)$$

and

$$A_0 e^{j(k_0 \cdot \sqrt{|\mu_r| \cdot |\epsilon_r|})x} \cdot e^{j\omega t} = A_0 e^{-k_0 \cdot \sqrt{|\mu_r| \cdot |\epsilon_r|}x} \cdot e^{j\omega t}. \quad (3)$$

This shows that the electromagnetic wave propagating along the negative  $x$ -component direction is evanescent. This means that the m-coupling resulting from the surface waves can be rejected.

### C. Antenna 2

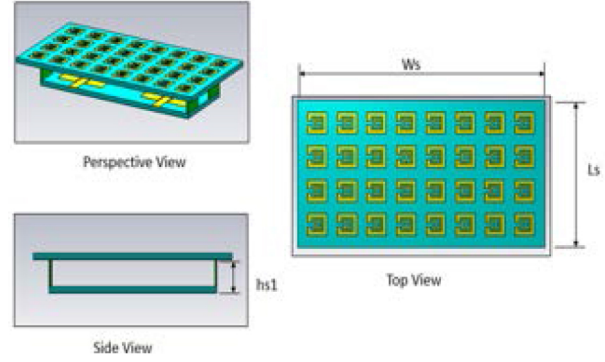
This design utilizes a single metasurface superstrate suspended above the antenna to reduce m-coupling between the two microstrip antenna elements. The metasurface superstrate is made up of periodic SRR unit cells printed on one side of an FR-4 substrate with a dielectric constant of 4.4 and a loss tangent of 0.002. The unit cells are placed at a distance ( $D$ ) from each other. The CST model of this design is depicted in Figure 5 (a). The top view and bottom view of fabricated Antenna 2 are shown in Figures 5 (b) and (c), respectively. The optimized design parameters of Antenna 2 are listed in Table 1.

### D. Antenna 3

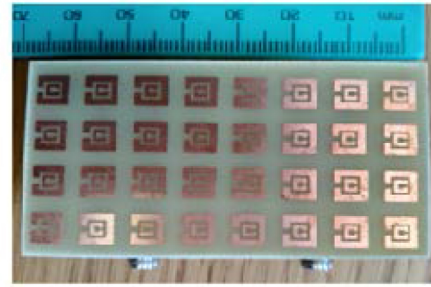
This design utilizes a double metasurface superstrate to reduce m-coupling between two microstrip antenna elements. The substrate ( $W_s \times L_s \times H$ ) is made up of  $4 \times 8$  SRR unit cells. Each metasurface substrate uses four dielectric poles to provide mechanical support. Figure 6 (a) depicts the CST model of Antenna 3. The top view of fabricated Antenna 3 and the combined fabricated Antenna 3 are shown in Figures 6 (b) and (c), respectively. The optimized dimensions of Antenna 3 are listed in Table 1.

## III. RESULTS AND DISCUSSION

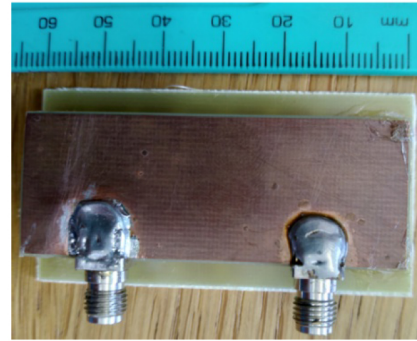
All the three antennas, which include the reference microstrip antenna (Antenna 1), the single suspended metasurface antenna (Antenna 2), and the double suspended metasurface substrate antenna (Antenna 3), are simulated using CST Microwave Studio. The antenna parameters which include reflection coefficient, radiation patterns, m-coupling, gain, and envelope correlation coefficient (ECC) are assessed, compared, and discussed. Figure 7 depicts the reflection coefficients of the antennas. From Figure 7, it can be seen that the reflection coefficient of Antenna 2 have significantly increased from  $-24$  to  $-14$  dB, which indicates that this antenna is not well matched, when compared to the reference antenna (Antenna 1). Additionally, a major bandwidth reduction of 49% at the frequency range of 6.05 – 6.15 GHz can be seen from the  $S_{11}$  parameter, while a bandwidth reduction of 43% can be seen from  $S_{22}$  parameter. Antenna 3 can be seen to



(a)



(b)



(c)

Fig. 5. Single suspended metasurface antenna (Antenna 2). (a) Antenna configuration. (b) Top view of fabricated Antenna 2. (c) Bottom view of fabricated Antenna 2.

be well matched with a bandwidth enhancement of 38% and 17% at the frequency range of 5.92 – 6.2 GHz for  $S_{11}$  and  $S_{22}$  parameters, respectively.

The m-coupling of the antennas is depicted in Figure 8. It can be seen that the m-coupling of Antenna 1 is drastically improved using the two mutual decoupling methods. Both Antenna 2 and Antenna 3 show m-coupling reduction over the entire bandwidth. Antenna 2 shows a maximum m-coupling of  $-60.6$  dB from  $-29$  dB, which is equivalent to a total m-coupling reduction of 31.6 dB. Antenna 3 shows a maximum

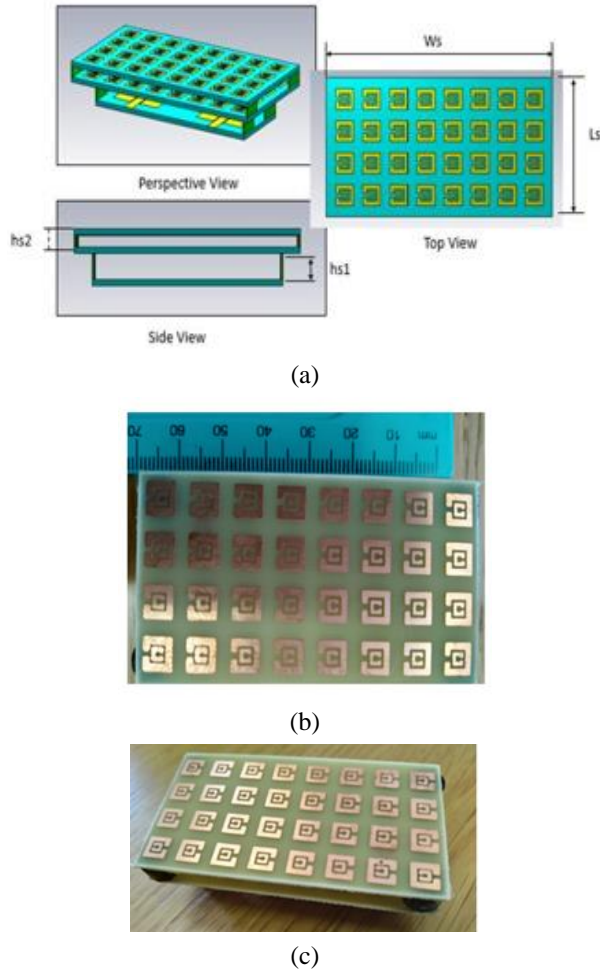


Fig. 6. Double suspended metasurface antenna (Antenna 3). (a) Antenna configuration. (b) Top view of fabricated Antenna 3. (c) Combined Antenna 3.

m-coupling reduction of  $-46$  dB from  $-24$  dB, which is equivalent to a total m-coupling reduction of 22 dB.

Figure 9 depicts the reflection coefficient of Antenna 2 with respect to various metasurface suspension heights ( $hs_1$ ). During the design of the metasurface-based antenna,  $hs_1$  is varied to obtain the optimal reflection coefficient and mutual coupling at the desired resonant frequency. It can be seen that varying  $hs_1$ , the resonant frequency and the  $S$ -parameters can be optimized.

Figures 10 (a)-(c) depict the simulated and measured  $S$ -parameters of Antenna 1, Antenna 2, and Antenna 3, respectively. Both simulated and measured results confirm the suitability of these antennas for mid-band 5G communication. Minor discrepancies can be seen between the simulated  $S$ -parameters and the measured  $S$ -parameters, and these discrepancies can be attributed to soldering residue, vector network analyzer calibration, fabrication, and assembly error.

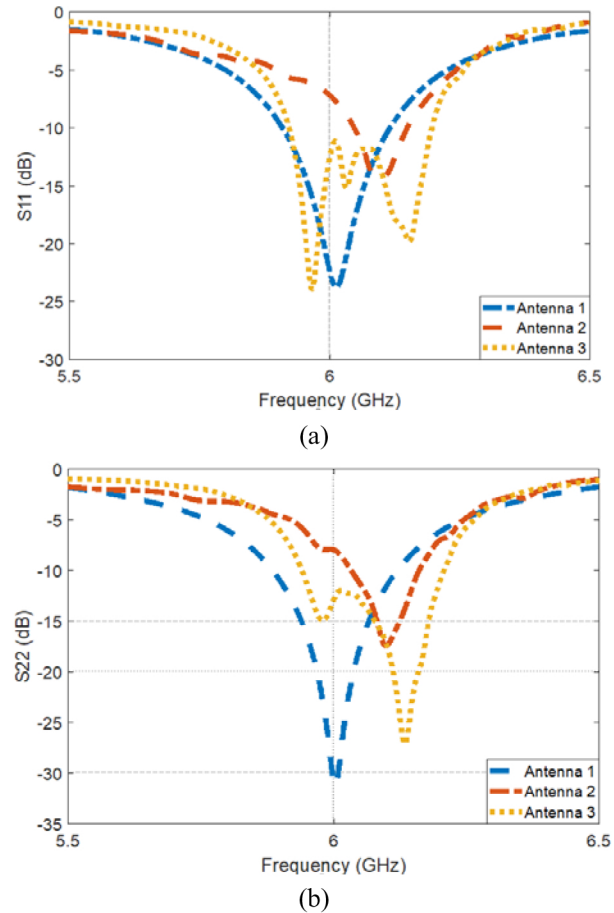


Fig. 7. Reflection coefficient of the antennas: (a) at port-1; (b) at port-2.

The radiation patterns of the antennas in the  $H$ -plane ( $\Phi = 0^\circ$ ) and  $E$ -plane ( $\Phi = 90^\circ$ ) at 6 GHz are depicted in Figure 11. Table 2 presents the radiation pattern parameters of the antennas which include main lobe direction, 3 dB beamwidth, total efficiency, radiation efficiency, maximum gain, and maximum directivity.

From Figure 11, it can be observed that the radiation pattern in the  $E$ -plane of Antenna 2 is highly distorted, while that of Antenna 3 can be seen to be more directive when compared to that of Antenna 1. This can also be seen that there is major gain increase of 2.09 dB. There is a slight decrease in the 3 dB beamwidth and an increase in maximum directivity of Antenna 3. Meanwhile, the  $H$ -plane radiation patterns of antennas are highly maintained. From Table 2, it can be observed that Antenna 2 shows a major decrease in total efficiency from 70% to 26%. This shows that Antenna 2 is poorly matched, while Antenna 3 also shows a decrease in total efficiency from 70% to 55% when compared to Antenna 1. This is still acceptable due to the fact that the efficiency is still greater than 50%.

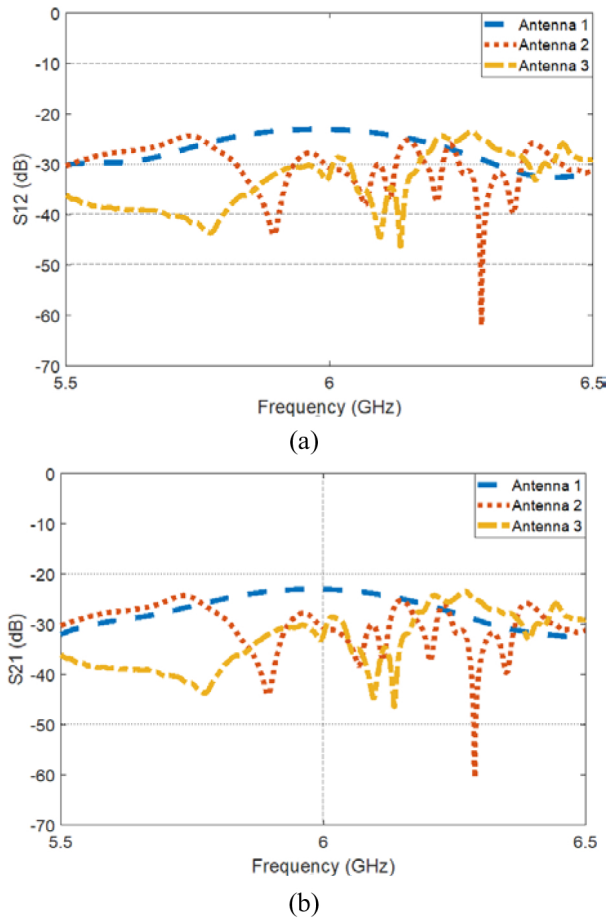


Fig. 8. M-coupling coefficient of the antennas. (a) S12. (b) S21.

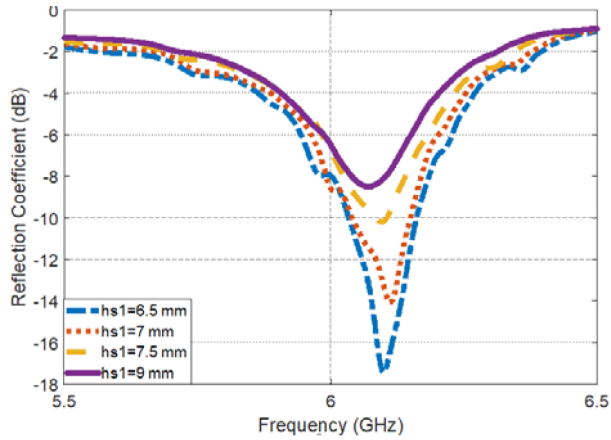


Fig. 9. Reflection coefficient of Antenna 2 with respect to different  $hs_1$  values.

Figure 12 depicts the realized gain for all three antennas. It can be observed that Antenna 2 shows a significant gain reduction over the entire bandwidth.

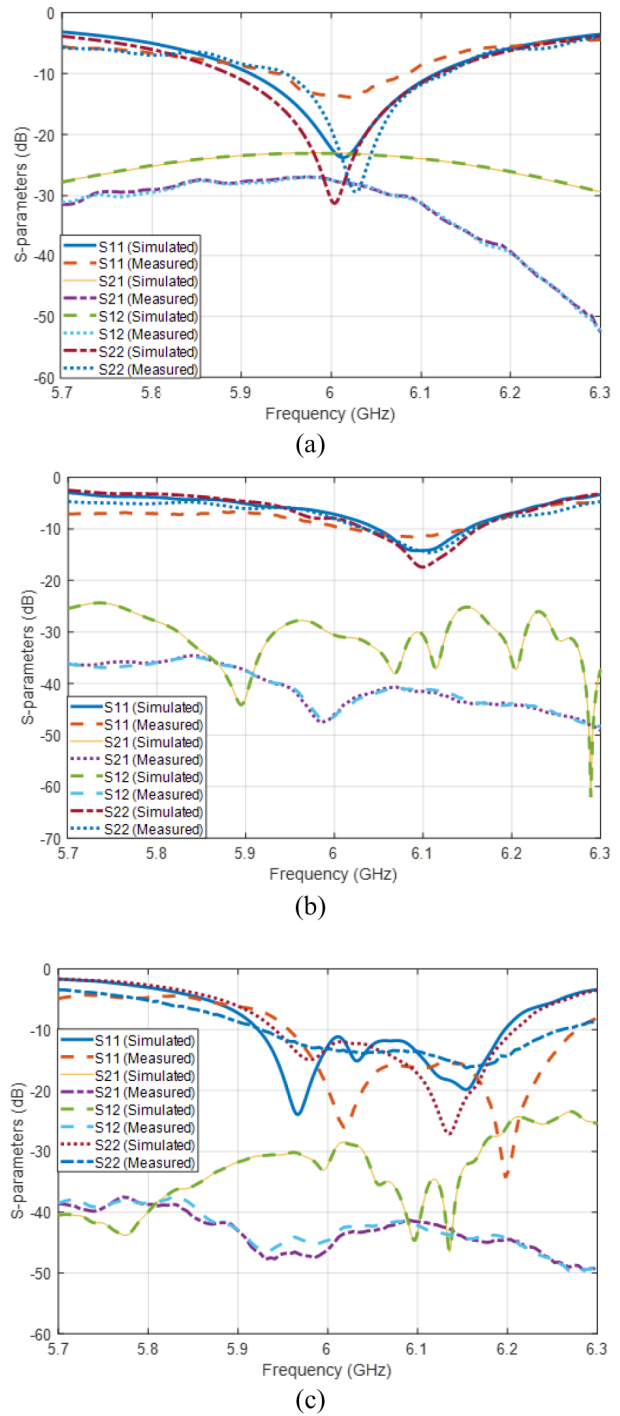


Fig. 10. Simulated and measured S-parameters of (a) Antenna 1, (b) Antenna 2, and (c) Antenna 3.

At 6 GHz, the gain of the antenna is reduced from 4.7 to 1.69 dB, which is equivalent to a gain reduction of 3.01 dB, while Antenna 3 shows a gain value 6.79 dB which is equivalent to a significant gain increase of 2.09 dB when compared to the reference antenna.

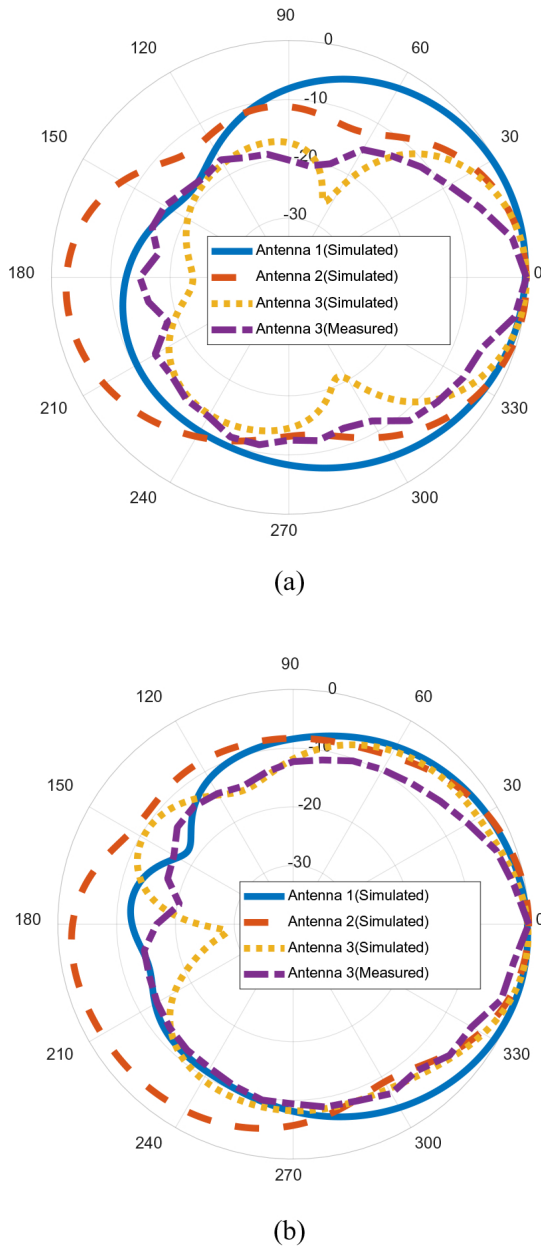


Fig. 11. Radiation patterns of the antennas. (a)  $H$ -plane. (b)  $E$ -plane.

This is attributed to the major m-coupling reduction that was achieved.

The ECC is also an important parameter to consider for any MIMO systems. It is also used to check the m-coupling in MIMO antenna systems. For a two-port MIMO antenna, the ECC can be calculated from  $S$ -parameters using the following equation [4]:

$$\rho_e = \frac{|S_{11}^* S_{12} + S_{21}^* S_{22}|}{(1 - (|S_{11}|^2 + |S_{21}|^2))(1 - (|S_{12}|^2 + |S_{22}|^2))}. \quad (4)$$

Table 2: Main lobe direction (in degrees), 3 dB beamwidth (in degrees), total efficiency, radiation efficiency, maximum gain (in dB), and maximum directivity (in dBi)

Antenna parameters	Antenna 1	Antenna 2	Antenna 3
Main lobe direction ( $\phi = 0^\circ$ )	11	1	6
Main lobe direction ( $\phi = 90^\circ$ )	12	3	0
3-dB Beamwidth ( $\phi = 0^\circ$ )	93.1	65.4	53.9
3-dB Beamwidth ( $\phi = 90^\circ$ )	99.1	61.9	50.1
Total efficiency	70%	26%	55%
Radiation efficiency	75%	32%	55%
Maximum gain	4,7	1.69	6.79
Maximum directivity	6.12	6.6	9.24

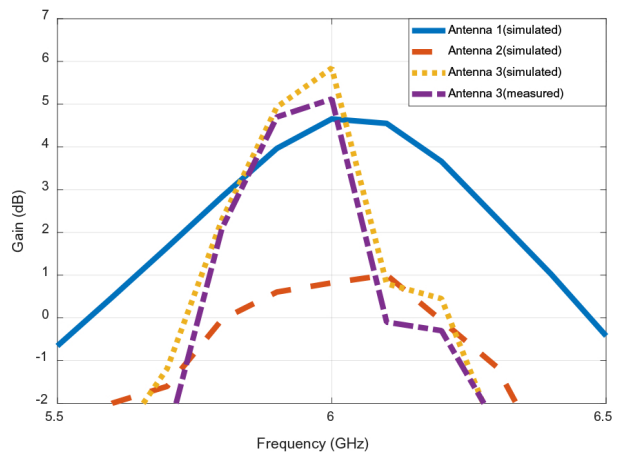


Fig. 12. Realized gain of the antennas.

Figure 13 depicts the ECCs of all three antennas. It can be seen that at 6 GHz, the ECC is less than 0.01, which demonstrates that two microstrip antenna elements are not correlated and that the m-coupling is well reduced.

Antenna 1 achieves maximum m-coupling reduction of 32 dB, while Antenna 2 achieves the maximum m-coupling reduction of 22 dB, 39% bandwidth increase, and a 2.09 dB gain enhancement. Table 3

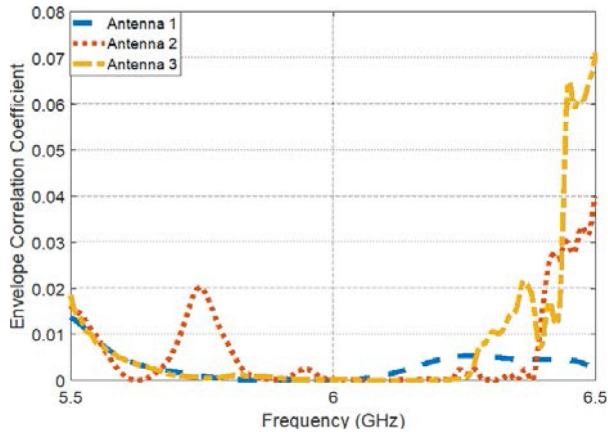


Fig. 13. Envelope correlation coefficient of the reference antenna and the proposed antennas.

Table 3: Comparison of the proposed antenna with the related works

Ref.	Size	Bandwidth	Method used	Edge to edge separation	m-coupling reduction	Gain enhancement
[1]	78 × 60 mm <sup>2</sup>	4.85–5.1 GHz (approx.)	MTM	0.25	5.5 dB	-
[9]	130 × 80 mm <sup>2</sup>	704–960 MHz, 1.7–2.17 GHz	DN	0.1	9 dB	-
[15]	480 × 160 mm <sup>2</sup> (approx.)	2.35–2.45 GHz	EBG	0.75	6 dB	-
[23]	140 × 100 mm <sup>2</sup>	11.82–12.2 GHz (approx.)	Parasitic patches	0.72	9 dB	-
[24]	43 × 43 mm <sup>2</sup>	2.27–2.35 GHz	DGS	0.116	10 dB	-
Proposed Antenna 3	65 × 33.862 mm <sup>2</sup>	5.92–6.2 GHz	MTS	0.29	22 dB	2.09 dB

compares the proposed metasurface-based antenna (Antenna 3) with the other decoupling methods. The techniques that are referenced and compared are the recent mutual decoupling techniques and they include DN, EBG, DGS, and MTM structures. It can be seen from the table that the proposed work is quite effective in reducing m-coupling when compared to other listed works. Moreover, the proposed structure also shows some other advantages when compared to other works such as bandwidth enhancement and gain improvement.

#### IV. CONCLUSION

In this paper, two metasurface superstrate-based antennas with reduced m-coupling between the ports have been proposed. The first metasurface-based antenna, i.e., Antenna 1 is constructed using a single metasurface superstrate that is suspended above the two radiating antenna elements. The second metasurface based antenna, i.e., Antenna 2 is constructed using a

double metasurface superstrate which is also suspended above the two antenna elements. The metasurface superstrate is made up of periodic SRRs printed on a FR-4 dielectric substrate. The metasurface is used for introducing a negative permeability medium, which converts the electromagnetic propagating waves into evanescent, hence rejecting m-coupling. It was shown that both antennas, i.e., Antenna 1 and Antenna 2 achieve significant m-coupling reduction over the entire bandwidth. Antenna 2 showed an m-coupling reduction of 31.6 dB, while Antenna 3 showed an m-coupling reduction of 22 dB, a 38% increase in bandwidth, and a gain enhancement of 2.09 dB. The low m-coupling, wide bandwidth, and high gain properties make Antenna 3 suitable for extended sub-6 GHz 5G wideband MIMO systems.

#### REFERENCES

- [1] M. M. Bait-Suwailam, O. F. Siddiqui, and O. M. Ramahi, "Mutual coupling reduction between microstrip patch antennas using slotted-complementary split-ring resonators," *IEEE Antennas Wirel. Propag. Lett.*, vol. 9, pp. 876-878, 2010. doi: 10.1109/LAWP.2010.2074175.
- [2] G. Expósito-Domínguez, J. M. Fernández-González, P. Padilla, and M. Sierra-Castañer, "EBG size reduction for low permittivity substrates," *Int. J. Antennas Propag.*, vol. 2012, pp. 1-8, 2012. doi: 10.1155/2012/106296.
- [3] D. Guha, S. Biswas, M. Biswas, J. Y. Siddiqui, and Y. M. M. Antar, "Concentric ring-shaped defected ground structures for microstrip applications," *IEEE Antennas Wirel. Propag. Lett.*, vol. 5, pp. 402-405, 2006. doi: 10.1109/LAWP.2006.880691.
- [4] B. C. Pan, W. X. Tang, M. Q. Qi, H. F. Ma, Z. Tao, and T. J. Cui, "Reduction of the spatially mutual coupling between dual-polarized patch antennas using coupled metamaterial slabs," *Sci. Rep.*, vol. 6, pp. 1-8, 2016. doi: 10.1038/srep30288.
- [5] M. Alibakhshikenari *et al.*, "A comprehensive survey on various decoupling mechanisms with focus on metamaterial and metasurface principles applicable to SAR and MIMO antenna systems," *IEEE Access*, vol. 8, pp. 192965-193004, 2020. doi: 10.1109/ACCESS.2020.3032826.
- [6] L. Zhao and K. Wu, "A decoupling technique for four-element symmetric arrays with reactively loaded dummy elements," *IEEE Trans. Antennas Propag.*, vol. 62, pp. 4416-4421, 2014. doi: 10.1109/TAP.2014.2326425
- [7] L. Zhao and K. Wu, "A dual-band coupled resonator decoupling network for two coupled antennas," *IEEE Antennas Propag. Mag.*, vol. 7,

- pp. 2843-2850, 2015. doi: 10.1109/TAP.2015.2421973
- [8] C. F. Ding et al., "Novel pattern-diversity-based decoupling method and its application to Multielement MIMO Antenna," *IEEE Trans. on Antennas and Propag.*, vol. 66, pp. 4976-4985, 2018. doi: 10.1109/TAP.2018.2851380
- [9] W. Chen and H. Lin, "LTE700 / WWAN MIMO antenna system integrated with decoupling structure for isolation improvement," *2014 IEEE Antennas and Prop. Society Int. Symp. (APSURSI)*, pp. 178-182, 2014.
- [10] M. S. Khan, A. Capobianco, A. I. Najam, I. Shoaib, E. Autizi, and M. Farhan, "Compact ultra-wideband diversity antenna with a floating parasitic digitated decoupling structure," *IET Microw., Antennas Propag.*, vol. 747, 2014. doi: 10.1049/iet-map.2013.0672
- [11] R. Xia, S. Qu, S. Member, P. Li, Q. Jiang, and Z. Nie, "An efficient decoupling feeding network for microstrip antenna array," *IEEE Antennas Wirel. Propag. Lett.*, vol. 14, pp. 871-874, 2015. doi: 10.1109/LAWP.2014.2380786
- [12] I. Nadeem and D. Choi, "Study on mutual coupling reduction technique for MIMO antennas," *IEEE Access*, vol. 7, pp. 563-586, 2019. doi: 10.1109/ACCESS.2018.2885558.
- [13] I. Mohamed and M. Abdalla, "Reduced size mushroom like EBG for antenna mutual coupling reduction," *32nd Natl. RADIO Sci. Conf.*, pp. 57-64, 2015. doi: 10.1109/NRSC.2015.7117815
- [14] V. Ionescu, M. Hnatiuc, and A. Topala, "Optimal design of mushroom-like EBG structures for antenna mutual coupling reduction in 2.4 GHz ISM band," *2015 E-Health Bioeng. Conf. EHB*, pp. 19-22, 2015. doi: 10.1109/EHB.2015.7391559.
- [15] F. Benykhlef and N. Boukli, "EBG structures for reduction of mutual coupling in patch antennas arrays," *J. Commun. Softw. Syst.*, vol. 13, pp. 9-14, 2017. doi: 10.24138/jcomss.v13i1.242.
- [16] X. Jiang et al., "A low mutual coupling MIMO antenna using EBG structures," *Prog. In Electrom. Research Symp.*, 2017. doi: 10.1109/PIERS.2017.8261823
- [17] A. Suntives and R. Abhari, "Miniaturization and isolation improvement of a multiple-patch antenna system using electromagnetic bandgap," *Microw. Opt. Technol. Lett.*, vol. 55, no. 7, pp. 1609-1612, 2013. doi: 10.1002/mop.27621
- [18] S. Ghosh, S. Member, T. Tran, and T. Lengoc, "Dual-layer EBG-based miniaturized multi-element," *IEEE Antennas Propag.*, vol. 62, pp. 3985-3997, 2014. doi: 10.1109/TAP.2014.2323410
- [19] B. Mohamadzade and M. Afsahi, "Mutual coupling reduction and gain enhancement in patch array antenna using a planar compact electromagnetic bandgap structure," *IET Microwaves, Antennas Propag.*, pp. 1719-1725, 2017. doi: 10.1049/iet-map.2017.0080.
- [20] J. Lee, S. Kim, and J. Jang, "Reduction of mutual coupling in planar multiple antenna by using 1-D EBG and SRR structures," *IEEE Trans. Antennas Propag.*, vol. 63, pp. 4194-4198, 2015. doi: 10.1109/TAP.2015.2447052
- [21] A. Dharmarajan et al, "A high gain UWB human face shaped MIMO microstrip printed antenna with high isolation," *Mult. Tools and App.*, 2022. doi: 0.1007/s11042-021-11827-7
- [22] F. Zulkifli, E. Rahardjo, and D. Hartanto, "Mutual coupling reduction using dumbbell defected ground structure for multiband microstrip antenna array," *Prog. Electromagn. Res. Lett.*, vol. 13, 29 2010. doi:10.2528/PIERL09102902
- [23] Q. C. Zhang, J. D. Zhang, and W. Wu, "Reduction of mutual coupling between cavity-backed slot antenna elements," *Prog. Electromagn. Res. C*, vol. 53, no. 27, 2014. doi: 10.2528/PIERC14052908.
- [24] C. Y. Chiu et al., "Reduction of mutual coupling between closely-packed antenna elements," *IEEE Trans. on Antennas and Prop.*, vol. 55, no. 6, pp. 1732-1738, 2007. doi: 10.1109/TAP.2007.898618
- [25] M. I. Ahmed, A. Sebak, E. A. Abdallah, and H. Elhennawy, "Mutual coupling reduction using defected ground structure (DGS) for array applications," *2012 15th Int. Symp. Antenna Technol. Appl. Electromagn.*, 2012. doi: 10.1109/ANTEM.2012.6262354.
- [26] G. Dadashzadeh, A. Dadgarpour, F. Jolani, and B. S. Virdee, "Mutual coupling suppression in closely spaced antennas," *IET Microwaves, Antennas Propag.*, vol. 5, 2011. doi: 10.1049/iet-map.2009.0564.
- [27] F. G. Zhu, J. Xu, and Q. Xu, "Reduction of mutual coupling between closely-packed antenna elements using defected ground structure," *Proc. - 2009 3rd IEEE Int. Symp. Microwave, Antenna, Propag. EMC Technol. Wirel. Commun.*, pp. 1-4, 2009. doi: 10.1109/MAPE.2009.5355659..
- [28] Q. L. Zhang, Y. T. Jin, J. Q. Feng, X. Lv, and L. M. Si, "Mutual coupling reduction of microstrip antenna array using metamaterial absorber," *2015 IEEE MTT-S Int. Microw. Work. Ser. Adv. Mater. Process. RF THz Appl.*, 2015. doi: 10.1109/IMWS-AMP.2015.7324947
- [29] H. Kondori, M. A. Mansouri-birjandi, and S. Tavakoli, "Reducing mutual coupling in microstrip

- array antenna using metamaterial spiral resonator,” *Int. J. Comput. Sci. Issues*, vol. 9, 2012.
- [30] A. A. Odhekar et al., “Mutual coupling reduction using metamaterial structure for closely spaced microstrip antennas,” *IJCA Proceedings on Int. Conf. on Comm. Technology*, pp. 9-11, 2013.
- [31] A. H. Jabire et al., “Metamaterial based design of compact UWB/MIMO monopoles antenna with characteristic mode analysis,” *Appl. Sci.*, vol. 11, no. 4, 1542, 2021. doi: 10.3390/app11041542
- [32] S. Luo and Y. Li, “A dual-band antenna array with mutual coupling reduction using 3D metamaterial structures,” *ISAP 2018 - 2018 Int. Symp. Antennas Propag.*, pp. 5-6, 2018.
- [33] K. Yu, Y. Li, and X. Liu, “Mutual coupling reduction of a MIMO antenna array using 3-D novel meta-material structures,” *The Applied Computational Electromagnetics Society (ACES) Journal*, vol. 33, 758, 2018.
- [34] P. Kumar and J. L. Masa-Campos, “Dual polarized monopole patch antennas for UWB applications with elimination of WLAN signals,” *Adv. Electromag.*, vol. 5, no. 1, pp. 46-52, 2016. doi: 10.7716/aem.v5i1.305
- [35] P. Kumar and J. L. Masa-Campos, “Dual polarized microstrip patch antennas for ultra wideband applications,” *Microw. and Opt. Tech. Lett.*, vol. 56, no. 9, pp. 2174-2179, 2014. doi: 10.1002/mop.28504
- [36] A. Kapoor et al., “Compact wideband-printed antenna for sub-6 GHz fifth-generation applications,” *Int J Smart Sensing Intell Syst*, vol. 13, pp. 1-10, 2020. doi: 10.21307/ijssis-2020-033
- [37] P. Kumar et al., “Flexible substrate based printed wearable antennas for wireless body area networks medical applications,” *Radioelectro. and Comm. Sys.*, vol. 64, no. 7, pp. 337-350, 2021. doi: 10.3103/S0735272721070013
- [38] R. Mishra et al., “Compact high gain multiband antenna based on split ring resonator and inverted F slots for 5G industry applications,” *The Applied Computational Electromagnetics Society (ACES) Journal*, vol. 36, no. 8, pp. 999-1007, 2021. doi: 10.47037/2021.ACES.J.360808999
- [39] T. O. Olawoye and P. Kumar, “A high gain microstrip patch antenna with slotted ground plane for sub-6 GHz 5G communications,” *Int. Conf. on Adv. in Big Data, Comp. and Data Comm. Sys.*, pp. 1-6, 2020. doi: 10.1109/icABCD49160.2020.9183820
- [40] B. W. Ngobese and P. Kumar, “A high gain microstrip patch array for 5 GHz WLAN applications,” *Adv. Electromag.*, vol. 7, no. 3, pp. 93-98, 2018. doi: 10.7716/aem.v7i3.783
- [41] “Unlicensed use of the 6 GHz Band, (report and order further notice of proposed rulemaking ET Docket NO. 18-295, GN Docket No. 17-1823),” Washington, D.C 20554, 2020.
- [42] “5G Spectrum public policy position,” (2016). [Online]. Available: <https://www.gsma.com/spectrum/wp-content/uploads/2016/06/GSMA-5G-Spectrum-PPP.pdf>
- [43] “5G frequency bands, channels for FR1 & FR2,” 2021. <https://www.electronics-notes.com/articles/connectivity/5g-mobile-wireless-cellular/frequency-bands-channels-fr1-fr2.ph>
- [44] D. Rowell, “The 6 GHz network?: Bigger channels, stronger signal, faster data,” 2020. <https://www.hpe.com/us/en/insights/articles/the-6-ghz-network-bigger-channels-stronger-signal-faster-data-2007.html>.
- [45] T. Lee, “What you should know about Wi-Fi 6 and the 6-GHz band,” 2019. <https://www.testandmeasurementtips.com/what-you-should-know-about-wi-fi-6-and-the-6-ghz-band/>.
- [46] N. Hussain et al., “A high-gain microstrip patch antenna using multiple dielectric superstrates for WLAN applications,” *The Applied Computational Electromagnetics Society (ACES) Journal*, vol. 35, no. 2, 2020.
- [47] R. S. Saxena et al., “Effects of dielectric substrate material microstrip antenna for limited band applications,” *Journal of Physics: Conference Series*, 012124, pp. 1-6, 2021. doi: 10.1088/1742-6596/2070/1/012124
- [48] N. Hussain and I. Park, “Performance of multiple-feed metasurface antennas with different numbers of patch cells and different substrate thicknesses,” *The Applied Computational Electromagnetics Society (ACES) Journal*, vol. 33, no. 1, pp. 49-55, 2018.
- [49] S. Dubazane et al., “Metasurface based MIMO microstrip antenna with reduced mutual coupling” *IEEE Africon*, pp. 1-7, 2021. doi: 10.1109/AFRICON51333.2021.9570916
- [50] L. N. Nguyen, “A new metasurface structure for bandwidth improvement of antenna array,” *The Applied Computational Electromagnetics Society (ACES) Journal*, vol. 36, no. 2, pp. 139-144, 2021.
- [51] Z. Wang, L. Zhao, Y. Cai, S. Zheng, and Y. Yin, “A meta-surface antenna array decoupling (MAAD) method for mutual coupling reduction in a MIMO antenna system,” *Sci. Rep.*, 2018. doi: 10.1038/s41598-018-21619-z
- [52] J. Tang et al., “A metasurface superstrate for mutual coupling reduction of large antenna arrays,” *IEEE Access*, vol. 8, 126859, 2020. doi: 10.1109/ACCESS.2020.3008162.



**Sthembile Promise Dubazane** was born in South Africa, on 27 June 1995. She received the B.Sc. degree in electronic engineering from the University of KwaZulu-Natal, South Africa, in 2017. She is currently working toward the M.Sc. degree in electronic engineering with the University of KwaZulu-Natal, South Africa.

She has a great passion for learning and hopes to conduct her Ph.D. degree studies in near future. Her research areas include antennas, MIMO systems, etc.



**Pradeep Kumar** received the bachelor's, M.Eng., and Ph.D. degrees in electronics and communication engineering in 2003, 2005, and 2009, respectively. He completed his postdoctoral studies from Autonomia University of Madrid, Spain.

He is currently working with the University of KwaZulu-Natal, South Africa. His current research areas include design and analysis of microstrip antennas, antenna arrays, wireless communications, etc.



**Thomas J. O. Afullo** received the B.Sc. degree (Hons.) in electrical engineering from the University of Nairobi, Kenya, in 1979, the M.Sc. degree in electrical engineering from the University of West Virginia, USA, in 1983, and the Ph.D. degree in electrical engineering from

Vrije Universiteit Brussel, Belgium, in 1989.

He is currently a Professor with the Discipline of Electrical, Electronic and Computer Engineering, University of KwaZulu-Natal, Durban, South Africa, and a former Academic Leader. He was with Kenya Post and Telecommunication Corporation as a Senior Executive Engineer from 1985 to 1986. He was a Senior Lecturer and the Head of the Department of Electrical and Communication Engineering, Moi University, Kenya, from 1991 to 1994. He was a Lecturer with the University of Botswana from 1996 to 2002, an Associate Professor with UDW/UKZN from 2003 to 2010, and has been a Professor with UKZN since 2012. His research interests include radio wave propagation, antenna design, cognitive radio, and power line communication.